

HUBBLE SPACE TELESCOPE IMAGING AND SPECTRAL ANALYSIS OF TWO BROWN DWARF BINARIES AT THE L DWARF/T DWARF TRANSITION

ADAM J. BURGASSER^{1,2}

Center for Astrophysics and Space Science, University of California San Diego, La Jolla, CA 92093, USA; aburgasser@ucsd.edu

DANIELLA C. BARDALEZ GAGLIUFFI¹

Massachusetts Institute of Technology, Kavli Institute for Astrophysics and Space Research, 77 Massachusetts Avenue, Cambridge, MA 02139, USA

AND

JOHN E. GIZIS

Department of Physics and Astronomy, University of Delaware, Newark, DE 19716, USA

Submitted to AJ on 23 August 2010; Accepted for publication 5 October 2010

ABSTRACT

We present a detailed examination of the brown dwarf multiples 2MASS J08503593+1057156 and 2MASS J17281150+3948593, both suspected of harboring components that straddle the L dwarf/T dwarf transition. Resolved photometry from *Hubble Space Telescope*/NICMOS show opposite trends in the relative colors of the components, with the secondary of 2MASS J0850+1057 being redder than its primary, while that of 2MASS J1728+3948 is bluer. We determine near-infrared component types by matching combined-light, near-infrared spectral data to binary templates, with component spectra scaled to resolved NICMOS and K_p photometry. Combinations of L7 + L6 for 2MASS J0850+1057 and L5 + L6.5 for 2MASS J1728+3948 are inferred. Remarkably, the primary of 2MASS J0850+1057 appears to have a later-type classification compared to its secondary, despite being 0.8–1.2 mag brighter in the near-infrared, while the primary of 2MASS J1728+3948 is unusually early for its combined-light optical classification. Comparison to absolute magnitude/spectral type trends also distinguishes these components, with 2MASS J0850+1057A being ≈ 1 mag brighter and 2MASS J1728+3948A ≈ 0.5 mag fainter than equivalently-classified field counterparts. We deduce that thick condensate clouds are likely responsible for the unusual properties of 2MASS J1728+3948A, while 2MASS J0850+1057A is either an inflated young brown dwarf or a tight unresolved binary, making it potentially part of a wide, low-mass, hierarchical quintuple system.

Subject headings: binaries: visual — stars: individual (2MASS J08503593+1057156, 2MASS J17281150+3948593) — stars: low mass, brown dwarfs

1. INTRODUCTION

The L dwarfs and the T dwarfs are the two lowest luminosity spectral classes of very low-mass stars and brown dwarfs known today, encompassing effective temperatures (T_{eff}) from ~ 2200 K down to ~ 600 K (Golimowski et al. 2004; Burningham et al. 2008; Stephens et al. 2009; see also Kirkpatrick 2005 and references therein). Spectroscopic studies of these sources reveal atmospheres that are remarkably diverse. L dwarfs having abundant molecular gas species and clouds of condensates in their photospheres, while T dwarfs have relatively cloud-free photospheres and more complex molecular gas species including CH₄, NH₃ and CO₂ (Oppenheimer et al. 1995; Roellig et al. 2004; Yamamura et al. 2010). Condensate cloud properties are believed responsible for near-infrared spectral and color variations among equivalently-classified L dwarfs (Knapp et al. 2004; Burgasser et al. 2008b;

Looper et al. 2008b), temporal variability in late-type dwarfs (Bailer-Jones & Mundt 2001; Gelino et al. 2002; Koen 2003; Artigau et al. 2009) and dramatic changes in the spectral energy distributions between the L dwarf and T dwarf classes (Leggett et al. 2000; Allard et al. 2001; Ackerman & Marley 2001; Burrows et al. 2006). Non-equilibrium chemistry and atmospheric circulation (Burrows et al. 2000; Lodders & Fegley 2002; Saumon et al. 2006) coupled with the complex processes of condensate grain formation, growth, circulation and evaporation (Helling & Woitke 2006; Helling et al. 2008) makes the formation, evolution and influence of condensate clouds in low-temperature atmospheres among the outstanding problems in brown dwarf astrophysics today.

The disappearance of photospheric condensates at the transition between the L dwarf and T dwarf classes is one particularly interesting aspect of brown dwarf clouds. This transition occurs over a narrow range of temperatures ($\Delta T_{eff} \approx 200$ K) and luminosities ($\Delta \log L_{bol}/L_{\odot} \approx 0.2$ dex; Kirkpatrick et al. 2000; Golimowski et al. 2004; Burgasser 2007a), and is accompanied by a temporary brightening at $1 \mu\text{m}$ (the “J-band bump”; Dahn et al. 2002; Tinney et al. 2003; Vrba et al. 2004) and enhanced rates of multiplicity (Burgasser et al. 2006c). These effects appear to arise from the rapid depletion of conden-

¹ Visiting Astronomer at the Infrared Telescope Facility, which is operated by the University of Hawaii under Cooperative Agreement no. NCC 5-538 with the National Aeronautics and Space Administration, Science Mission Directorate, Planetary Astronomy Program.

² Hellman Fellow.

sate clouds at the L dwarf/T dwarf transition (Liu et al. 2006; Burgasser 2007a), although the driving mechanism for that depletion is inadequately explained by current cloud models (Burrows et al. 2006; Cushing et al. 2008; Saumon & Marley 2008). Whether arising from the fragmentation of cloud structures (Ackerman & Marley 2001; Burgasser et al. 2002), a sudden increase in sedimentation efficiency (Knapp et al. 2004; Stephens et al. 2009) or some other process remains unclear, but cloud depletion at the L dwarf/T dwarf transition has important implications on cloud evolution in other low-temperature atmospheres, such as those of extrasolar planets (Fortney 2005).

Coeval and cospatial multiples are important laboratories for studying this transition, eliminating dependencies on age, composition and distance. So-called “flux-reversal” binaries, whose components straddle the L dwarf/T dwarf transition, have verified the 1 μm brightening as an intrinsic aspect of brown dwarf evolution (Gizis et al. 2003; Cruz et al. 2004; Burgasser et al. 2006c; Liu et al. 2006; Looper et al. 2008a). Yet resolved spectroscopy of the components of these systems has been difficult to obtain, due largely to the close separations typical of brown dwarf multiples ($a \lesssim 20$ AU; Allen 2007). In this article, we present a comprehensive analysis of two binaries whose components are suspected to straddle this transition: 2MASS J08503593+1057156 (hereafter 2MASS J0850+1057) and 2MASS J17281150+3948593 (hereafter 2MASS J1728+3948). Both were resolved with the *Hubble Space Telescope* (HST) Wide Field Planetary Camera 2 (WFPC2; Reid et al. 2001b; Gizis et al. 2003) and noted as potential L dwarf/T dwarf transition binaries based on their photometric properties and late (combined-light) systemic spectral types of L6 and L7, respectively. Here we combine resolved near-infrared photometry obtained with the HST/Near Infrared Camera and Multi-Object Spectrometer (NICMOS) and ground-based laser guide star adaptive optics (LGSAO) imaging with combined-light, near-infrared spectroscopy to infer component spectral types, colors and absolute magnitudes. Observations are described in Section 2. In Section 3 we describe point spread function (PSF) fitting of the HST data that yield relative fluxes for each binary in five spectral bands spanning 1.0–1.8 μm . In Section 4 we describe our spectral fitting procedure and determine component classifications, colors and absolute magnitudes. In Section 5 we compare these measures to current absolute magnitude/spectral type and absolute magnitude/color trends. In Section 6 we discuss our results in the context of cloud evolution at the L dwarf/T dwarf transition, and explore the possibility of higher-order multiplicity in the case of 2MASS J0850+1057. Results are summarized in Section 7.

2. OBSERVATIONS

2.1. Targets

The empirical properties of the two binaries examined here are summarized in Table 1. 2MASS J0850+1057 was initially identified in the Two Micron All Sky Survey (2MASS; Skrutskie et al. 2006) by Kirkpatrick et al. (1999), and selected to be the prototype for the L6

spectral subclass. Its optical spectrum exhibits 6708 Å Li I absorption, indicating component masses below $\sim 0.06 M_{\odot}$ (Rebolo et al. 1992; Magazzu et al. 1993). This source was resolved as a $0''.16$ binary system by Reid et al. (2001b) with HST/WFPC2, and has been subsequently confirmed as a common proper motion pair from multi-epoch HST and LGSAO observations (Bouy et al. 2008; Konopacky et al. 2010). The large difference in component brightnesses in the WFPC2 F814W band ($\Delta F814W = 1.47 \pm 0.09$; Bouy et al. 2003) has suggested a late-type L or early-type T dwarf secondary, although this component has been a persistent outlier in color magnitude diagrams. Astrometric parallax measurements by Dahn et al. (2002) and Vrba et al. (2004) find discrepant distances of 25.6 ± 2.3 pc and 38 ± 6 pc, differing by nearly 2σ . Faherty et al. (2010) identified an unrelated background source that may have skewed the Dahn et al. (2002) astrometric measurements, and report a preliminary parallax that is intermediate between these two values. We adopt the Vrba et al. (2004) for this study, as was also used by Konopacky et al. (2010). Faherty et al. (2010) also identified a widely-separated, common proper motion and common distance companion to 2MASS J0850+1057, the M5 + M6 binary NLTT 20346AB at a projected separation of $4''.1$ (7700 AU). H α and X-ray emission in these M dwarfs, coupled with Li I absorption in 2MASS J0850+1057, indicate a relatively young age of 0.25–1.5 Gyr for the combined system, and relatively low masses for the 2MASS J0850+1057 components: $0.04 \pm 0.02 M_{\odot}$ and $0.03 \pm 0.01 M_{\odot}$ based on evolutionary models (Faherty et al. 2010). These mass estimates are consistent with weak empirical constraints by Konopacky et al. (2010), $M_{\text{total}} = 0.2 \pm 0.2 M_{\odot}$, as inferred from incomplete astrometric monitoring of its orbit.

2MASS J1728+3948 was also identified in 2MASS by Kirkpatrick et al. (2000) and classified L7 based on its optical spectrum. This source shows no indication of Li I absorption and hence its primary is inferred to have a mass greater than $0.06 M_{\odot}$. Gizis et al. (2003) and Bouy et al. (2003) identified this system as a $0''.13$ binary based on HST/WFPC2 observations. The former study found the “secondary” to be fainter in the F814W band and brighter in the F1042M band, the first reported example of a L/T flux reversal binary. Multi-epoch HST and LGSAO observations reported in Bouy et al. (2008) and Konopacky et al. (2010) have verified the common proper motion of the components, with the latter study finding an orbital period of 31 ± 12 yr, semimajor axis of 5.3 ± 0.8 AU (based on the parallax distance measurement of 24.1 ± 1.9 pc; Vrba et al. 2004) and total system mass of $0.15^{+0.25}_{-0.04} M_{\odot}$. However, like 2MASS J0850+1057, the orbit of this system has not been fully sampled. Assuming a primary temperature of ≈ 1450 K based on the combined light optical spectral type (Stephens et al. 2009; Konopacky et al. 2010), the absence of Li I indicates a system age of at least 1.5 Gyr, according to the evolutionary models of Burrows et al. (1997) and Saumon & Marley (2008).

2.2. IRTF/SpeX Observations

Low resolution near-infrared spectral data for 2MASS J0850+1057 and 2MASS J1728+3948 were

TABLE 1
 PROPERTIES OF 2MASS J08503593+1057156 AND 2MASS J17281150+3948593

Parameter	2MASS J0850+1057	2MASS J1728+3948	Reference
Optical Spectral Type ^a	L6	L7	1,2
NIR Spectral Type ^{a,b}	L7±2	L6±1	3
MKO <i>J</i>	16.20±0.03	15.90±0.08 ^c	3,4
MKO <i>J - K</i>	1.85±0.04	2.01±0.09 ^c	3,4
Distance (pc)	38±6 ^d	24.1±1.9	5
<i>V</i> _{tan} (km s ⁻¹)	26.6±4.5	5.1±0.9	5
Separation (mas) ^e	157±3	131±3	6
(AU)	6.0±0.9	3.2±0.3	5,6
Position Angle (°) ^e	114.7±0.3	27.6±1.2	6
$\Delta F814W$	1.47±0.09	0.37±0.04 ^f	6,7
$\Delta F1042M$...	-0.25±0.14	7
ΔK_p ^g	0.78±0.07	0.63±0.03	8
Li I? ^h	Yes	No	1,2
Age (Gyr) ^h	0.25–1.5	≥1.5	3,9
Combined Mass (M _⊙) ⁱ	0.2±0.2	0.15 ^{+0.25} _{-0.04}	8

REFERENCES. — (1) Kirkpatrick et al. (1999); (2) Kirkpatrick et al. (2000); (3) This paper; (4) Skrutskie et al. (2006); (5) Vrba et al. (2004); (6) Bouy et al. (2003); (7) Gizis et al. (2003); (8) Konopacky et al. (2010); (9) Faherty et al. (2010).

^a Classification of combined light spectra.

^b Based on spectral indices measured from SpeX spectroscopy; see Section 2.2 and Table 2.

^c Synthesized from 2MASS photometry and spectrophotometric filter corrections computed from the spectrum shown in Figure 1.

^d Dahn et al. (2002) and Faherty et al. (2010) report parallactic distances of 25.6±2.3 pc and 29±7 pc for 2MASS J0850+1057, both closer than the Vrba et al. (2004) measurement. The Faherty et al. study propose that the differences may arise from a contaminant background source skewing center-of-light measurements. We adopt the Vrba et al. distance for consistency, and note that an uncertainty-weighted mean of this measurement and that of Faherty et al., 36±5 pc, is fully consistent with the adopted value.

^e At epoch 2000 February 1 (UT) for 2MASS J0850+1057 and 2000 August 12 (UT) from 2MASS J1728+3948.

^f Bouy et al. (2003) report $\Delta F814W = 0.66±0.11$ for this system based on the same dataset, a 2.5 σ difference.

^g Uncertainty-weighted averages of multi-epoch flux ratio measurements from Konopacky et al. (2010), using both statistical and PSF-matching systematic uncertainties.

^h Based on presence/absence of Li I, and for 2MASS J0850+1057 activity diagnostics in its co-moving companion NLTT 20346AB (Faherty et al. 2010).

ⁱ Based on partial coverage of astrometric orbits.

obtained with the 3m NASA Infrared Telescope Facility (IRTF) SpeX spectrograph (Rayner et al. 2003) on 2008 January 8 (UT) and 2006 August 21 (UT), respectively. Conditions on both nights were mostly clear, with light cirrus during the 2006 August observations; seeing was $\sim 0''.6$ at *J*-band in both observations. We employed the prism-dispersed mode of SpeX which provides 0.75–2.5 μm continuous spectroscopy at a resolution $\lambda/\Delta\lambda \approx 120$ for the $0''.5$ slit, and dispersion of 20–30 \AA pixel⁻¹. The slit was aligned to the parallactic angle in all observations. 2MASS J0850+1057 was observed at an airmass of 1.13, with four exposures of 150 s each obtained in an ABBA dither pattern along the slit. 2MASS J1728+3948 was observed in a similar manner, at an airmass of 1.06 and with four exposures of 180 s each. After each target observation, A0 V stars HD 74721 ($V = 8.71$) and HD 164899 ($V = 7.91$) were observed with identical instrument settings and at a similar airmass for telluric absorption and flux calibration. These were followed by internal flat field and Ar arc lamps for pixel response and wavelength calibration. Data were reduced using the SpeXtool package, version 3.3 (Vacca et al. 2003; Cushing et al. 2004) using standard settings; see Burgasser & McElwain (2006) for

details.

The reduced spectra for both sources are shown in Figure 1. The data exhibit classic signatures of L dwarf near-infrared spectra, including a steep 0.8–1.2 μm spectral slope; FeH absorption at 1.0 μm ; unresolved K I and Na I doublets at 1.13, 1.17 and 1.22 μm ; deep H₂O absorption bands centered at 1.4 and 1.9 μm ; and CO absorption at 2.3 μm (Reid et al. 2001a; McLean et al. 2003; Cushing et al. 2005). Their overall near-infrared spectral energy distributions are fairly red, consistent with their *J - K_s* colors and indicative of cloud opacity capping the 1.25 μm and 1.65 μm spectral peaks (Ackerman & Marley 2001). There is no obvious indication of CH₄ absorption at either 1.6 μm or 2.2 μm , commonly seen in the combined light spectra of L dwarf/T dwarf pairs (e.g., Cruz et al. 2004; Burgasser 2007b).

We derived near-infrared spectral types for these sources using the H₂O-J, H₂O-H and CH₄-K spectral indices defined in Burgasser et al. (2006b), and the index-spectral type relations defined in Burgasser (2007a) which have a typical scatter of ~ 1 subtype for L0–L8 dwarfs. Values are reported in Table 2. The inferred near-infrared types are L7±2 for 2MASS J0850+1057 and L6±1 for 2MASS J1728+3948. These types are

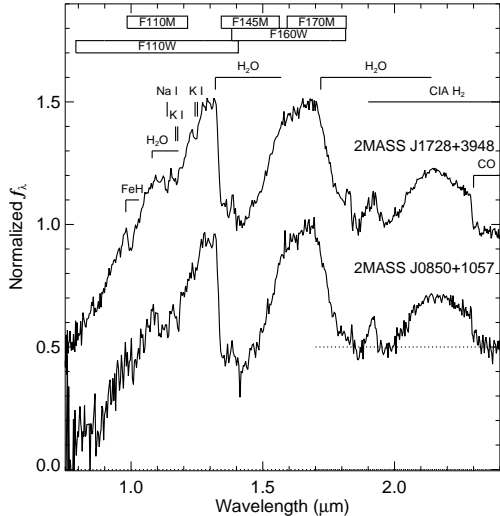


FIG. 1.— Near-infrared spectra of 2MASS J0850+1057 (bottom) and 2MASS J1728+3948 (top) obtained with IRTF/Spex. Data are normalized at the $1.3 \mu\text{m}$ spectral peaks, with the spectrum of 2MASS J1728+3948 vertically offset for clarity (dotted line). Major spectral features characteristic of L dwarf spectra are labeled. Also indicated are the wavelength ranges spanned by the F110M, F110W, F145M, F160W and F170M HST/NICMOS filters.

TABLE 2
NEAR-INFRARED SPECTRAL INDEX MEASUREMENTS

Index	2MASS J0850+1057		2MASS J1728+3948	
	Value	SpT	Value	SpT
H ₂ O-J	0.673±0.014	L8.0±0.4	0.712±0.009	L6.9±0.3
H ₂ O-H	0.652±0.010	L8.2±0.4	0.723±0.005	L5.6±0.2
CH ₄ -K	0.987±0.009	L4.8±0.3	0.955±0.004	L5.9±0.2
Mean SpT		L7±2		L6±1

NOTE. — Spectral indices and index-spectral type relations are defined in Burgasser et al. (2006b) and Burgasser (2007a), respectively. Mean values and uncertainties in indices and index types were calculated from 1000 realizations of each spectrum randomly varied according to its noise spectrum. Overall mean types and their uncertainties are the average and scatter of the index types, rounded off to the nearest whole subtype.

later and earlier than the reported optical types for these sources, respectively, albeit consistent within the uncertainties. The larger uncertainty in the near-infrared spectral type of 2MASS J0850+1057 is driven by a discrepant CH₄-K index value, which indicates an L5 spectral type as compared to L8 from the H₂O indices. This difference may be related to the multiplicity of this system, or its young age and the corresponding low surface gravity of its components.

2.3. HST/NICMOS Observations

Both sources were observed in single orbits with the HST/NICMOS NIC1 camera as part of program GO-9843 (PI Gizis). 2MASS J0850+1057 was observed on 2003 November 9 (UT) and 2MASS J1728+3948 on 2003 September 7 (UT). NIC1 is the highest-resolution camera on NICMOS with pixel scale $0''.043$ and field of view $11'' \times 11''$, providing a well-sampled PSF down to the diffraction limit at $1 \mu\text{m}$. Both sources were observed through the wide-band filters F110W ($\lambda_c = 1.025 \mu\text{m}$,

$\Delta\lambda = 0.6 \mu\text{m}$) and F160W ($\lambda_c = 1.55 \mu\text{m}$, $\Delta\lambda = 0.4 \mu\text{m}$), and the medium-band filters F110M ($\lambda_c = 1.1 \mu\text{m}$, $\Delta\lambda = 0.2 \mu\text{m}$), F145M ($\lambda_c = 1.45 \mu\text{m}$, $\Delta\lambda = 0.2 \mu\text{m}$), and F170M ($\lambda_c = 1.7 \mu\text{m}$, $\Delta\lambda = 0.2 \mu\text{m}$). As shown in Figure 1, the F110W and F160W filters sample the prominent J and H flux peaks of late-type L and T dwarf spectra, while the F110M, F145M and F170M filters sample the $1.1 \mu\text{m}$ H₂O, $1.4 \mu\text{m}$ H₂O and $1.6 \mu\text{m}$ CH₄ absorption bands, respectively. These filter combinations provide discriminating colors for late-type L and T dwarfs (e.g., Burgasser et al. 2006c; Reid et al. 2006; Figure 3). All data were acquired in MULTIACCUM mode, with two dithered exposures ($1''.5$ step) obtained in each filter. Total integration times for each source were 256 s in F110W and F110M (2MASS J1728+3948 was observed for 288 s in F110M), 320 s in F160W, 704 s in F170M and 832 s in F145M. Integrations were longest with the F145M filter because of the deep H₂O absorption present at these wavelengths.

Raw images were reduced by standard pipeline processing (CALNICA, Bushouse 1997) using calibration images (inflight and model reference files, circa 2002) and photometric keywords (post-cryogenic) current as of February 2008. CALNICA reduction includes analog-to-digital correction, subtraction of bias and dark current frames, linearity correction, correction for readout artifacts (the “bars” anomaly), division by an appropriate flat field image, photometric calibration, cosmic ray identification, and combination of MULTIACCUM frames into a single calibrated image. No correction was made for the temperature dependence of the dark and flat-field reference files. These basic calibrated images (two images per filter per object) were used for the analysis.

Figure 2 displays subsections of the calibrated imaging data for each binary in the five filter bands. Two components are resolved in each image, although the increase in PSF size in the longer wavelength data results in better PSF separation in the F110M and F110W images as compared to the F170M images. There are notable differences in the relative component fluxes between these two sources. The eastern component of 2MASS J0850+1057 is significantly fainter than the western component in all five filter bands, while the two components of 2MASS J1728+3948 are roughly equal in brightness. We measured aperture photometry for the combined light of each source using the IRAF³ PHOT routine, employing a 15 pixel radius aperture centered on the brightest component and a 20-25 pixel annulus to measure the median background. Count rates were converted to Vega magnitudes on the CIT system using photometric conversion parameters listed in the NICMOS Data Handbook version 8.0⁴, but without applying aperture corrections. Values are listed in Table 3, where the uncertainties include shot noise and background uncertainties, as well as a standard 5% calibration uncertainty. Relative photometric measurements are discussed below.

3. HST/NICMOS PSF FITTING ANALYSIS

³ Image Reduction and Analysis Facility (IRAF; Tody 1986) is distributed by the National Optical Astronomy Observatories, which are operated by the Association of Universities for Research in Astronomy, Inc., under cooperative agreement with the National Science Foundation.

⁴ <http://www.stsci.edu/hst/nicmos/documents/handbooks/DataHandbookv8>

TABLE 3
HST/NICMOS PHOTOMETRY AND ASTROMETRY

Parameter	2MASS J0850+1057				2MASS J1728+3948			
	AB	Δ	A	B	AB	Δ	A	B
Epoch	2003 Nov 9				2003 Sep 7			
F110W	17.38±0.07	1.15±0.03	17.70±0.07	18.99±0.08	16.76±0.05	0.322±0.015	17.36±0.05	17.68±0.05
F110M	17.49±0.06	1.176±0.015	17.81±0.06	18.99±0.08	16.81±0.07	0.25±0.03	17.44±0.07	17.69±0.07
F145M	16.48±0.05	1.000±0.015	16.84±0.05	17.84±0.05	15.77±0.05	0.517±0.014	16.29±0.05	16.81±0.05
F160W	15.70±0.05	0.90±0.05	16.09±0.05	16.99±0.06	15.08±0.05	0.461±0.016	15.63±0.05	16.09±0.05
F170M	15.36±0.05	0.89±0.07	15.76±0.05	16.65±0.07	14.77±0.05	0.462±0.014	15.32±0.05	15.78±0.05
F110W-F160W	1.68±0.09	...	1.61±0.09	1.86±0.10	1.68±0.07	...	1.74±0.07	1.60±0.07
F110W-F170M	2.02±0.09	...	1.95±0.09	2.21±0.10	1.99±0.07	...	2.05±0.07	1.91±0.07
ρ (mas)		132±5				158±5		
(AU)		5.0±0.8				3.8±0.3		
PA (°)		126.1±0.7				68.0±0.5		

NOTE. — Photometry in Vega magnitudes on the CIT system based on conversions given in the NICMOS Data Handbook version 8.0.

3.1. Method

Relative photometry for the components of each binary were determined using a PSF-fitting algorithm similar to that described in Burgasser et al. (2006c). Models for each binary image were generated using PSFs calculated with the *Tiny Tim* package, version 6.3 (Krist 1995). PSFs were generated for each filter passband (assuming post-cryocooler aberrations for NIC1), and at two pointing positions to account for mirror zonal errors. The SpeX spectra of each source were used as templates for calculating filter passband effects. Individual PSF models were generated for a subimage size of $3'' \times 3''$, which was resampled at ten times the original resolution to allow for subpixel offsets.

A binary PSF model for each NICMOS image was determined using an iterative image fitting algorithm that finds optimal positions and relative fluxes. Initial guesses were found using a simple peak detection algorithm and single-PSF subtraction on a $3'' \times 3''$ subframe of the data image centered on the binary. We then varied the primary position, secondary position, primary flux and secondary flux, in that order, to minimize the statistic

$$S^2 = \sum_i \sum_j W_{ij} (D_{ij} - M_{ij} - \langle D - M \rangle_{ij})^2 \quad (1)$$

where D is the data subframe, M is the model image, W is a masking image used to exclude bad pixels ($W = 0$ for bad pixels), $\langle D - M \rangle$ is the mean difference (to account for residual background flux in the data) and the sum is performed over all pixels. The iteration step in position was set at 0.1 pixels (4.3 mas) in accord with the subsampling of the PSF model; the iteration in flux values was 1%. Iterations were performed in a hierarchical recursive loop, and ceased when the fractional decrease in S^2 was less than 10^{-8} for all parameters. For each source, we adopted as our final relative flux values the mean of the two pointing frames in each filter band, and uncertainties include the difference in individual measurements and a 1% flux sampling uncertainty. Final separations and position angles⁵ were adopted as the mean

⁵ The position angle is measured east of north, assuming a vector that points from primary to secondary. The HST roll angles at the time of observation are included in the values, assumed to be accurate to within $0^\circ 003$ (Bouy et al. 2008).

of all frames, with uncertainties incorporating measurement scatter and a 0.1 pixel sampling uncertainty.

The close separation and overlapping PSFs of the components of these two systems initially raised concerns that fitting biases for the longer-wavelength images (e.g., F170M) could lead to skewed component photometry and colors. This was of particular concern for 2MASS J0850+1057, whose components have a larger difference in brightness. To test our fitting program, we performed an identical analysis with simulated binary images generated from the model PSFs. The simulated images were constructed to have the same component positions and relative magnitudes as determined from the PSF fitting (see below) as well as relative magnitudes inferred from unconstrained spectral fits (see Section 4.1). In both cases, the fitting algorithm reproduced the input relative magnitudes in all filter bands to within 0.01 mag, even for the F170M images of 2MASS J0850+1057.

3.2. Results

Table 3 summarizes the results of the PSF fitting analysis and all of the NICMOS photometry. We find separations and position angles that are consistent to within 1.5σ of those measured by Bouy et al. (2008) using the same NICMOS data. The relative magnitudes are all positive, indicating that the primary components are brighter than the secondary components at these wavelengths for both sources. Relative component brightnesses show distinct trends. For 2MASS J0850+1057, relative magnitudes decrease toward longer wavelengths, from $\Delta F_{110M} = 1.176 \pm 0.015$ to $\Delta F_{170M} = 0.89 \pm 0.07$, indicating a secondary that is redder than the primary. This is confirmed by the redder broadband color of the secondary, $F_{110W} - F_{160W} = 1.61 \pm 0.09$ and 1.86 ± 0.10 for 2MASS J0850+1057A and 2MASS J0850+1057B, respectively. In contrast, the relative magnitudes of 2MASS J1728+3948 generally increase toward longer wavelengths (with the exception of the F145M band) indicating a bluer secondary. This trend is also seen in resolved JHK_p photometry for 2MASS J1728+3948 by Konopacky et al. (2010).

Figure 3 compares the colors of the 2MASS J0850+1057 and 2MASS J1728+3948 components to spectrophotometric estimates calculated from L2–T6 SpeX spectral templates (Section 4.1). In gen-

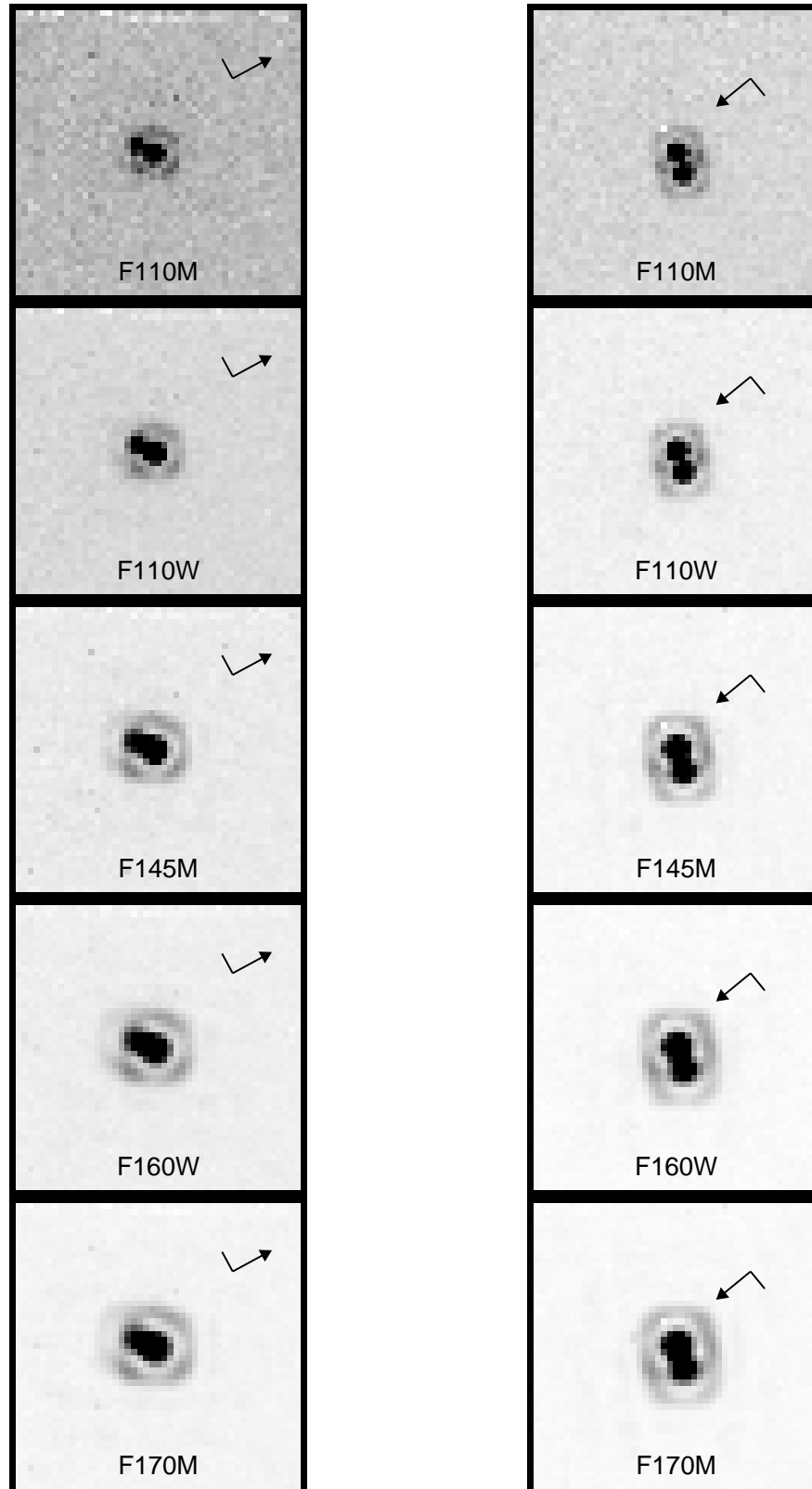


FIG. 2.— HST/NICMOS images of 2MASS J0850+1057 (left) and 2MASS J1728+3948 (right) in the F110M, F110W, F145M, F160W and F170M filters (top to bottom). Each image is $2''.15$ (50 NIC1 pixels) on a side with orientations on the sky indicated by the arrows (head points north, stem points east).

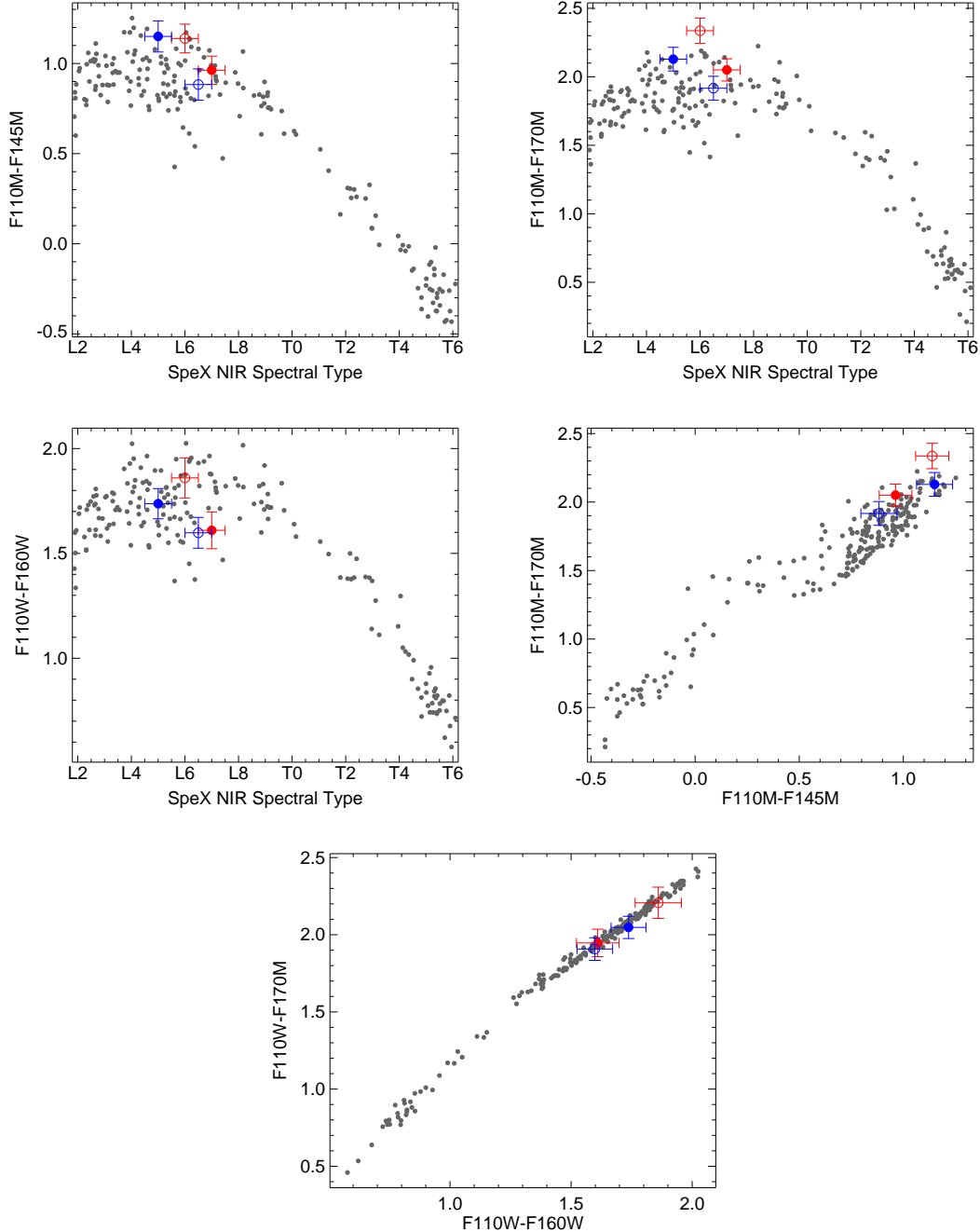


FIG. 3.— Segregation of L and T dwarfs with NICMOS photometry, based on spectrophotometric colors computed from SpeX templates. The first three panels show trends in narrow-band F110M-F145M and F110M-F170M colors and broadband F110W-F160W color with near-infrared (SpeX-based) spectral type. The last two panels compare color pairs F110M-F145M versus F110M-F170M and F110W-F170M versus F110W-F160W. Measured colors for the individual components of 2MASS J0850+1057 and 2MASS J1728+3948 are indicated in red and blue, respectively, with the primaries (secondaries) indicated by solid (open) circles. In the first three panels, the components are shown with at their inferred near-infrared spectral types based on the spectral fitting analysis described in Section 4.

eral, the components span the full range of colors seen in the L dwarf templates, although 2MASS J0850+1057B and (to lesser degree) 2MASS J1728+3948A are notably redder in both broadband and narrow-band colors. F110M-F145M and F110M-F170M colors, sampling $1.4 \mu\text{m}$ H₂O and $1.6 \mu\text{m}$ CH₄ features, indicate that none of the components have spectral types T0 or later; i.e., they are all L dwarfs. NICMOS colors alone are unable to distinguish L subtypes for the individual

components. They are, however, cleanly segregated in F110W-F170M and F110W-F160W colors, which are correlated for the L and T dwarf templates. The binary components follow a sequence of 2MASS J1728+3948B, 2MASS J0850+1057A, 2MASS J1728+3948A and 2MASS J0850+1057B in this color-color plot, in order of increasing F110W-F170M and F110W-F160W colors.

4. SPECTRAL TEMPLATE FITTING ANALYSIS

4.1. Method

To infer the component near-infrared spectral types of 2MASS J0850+1057 and 2MASS J1728+3948, we compared their combined-light SpeX spectra to a suite of empirical binary templates scaled to the observed relative photometry. We followed a procedure similar to that described in Burgasser et al. (2006c), drawing from a uniform sample of low-resolution, high signal-to-noise SpeX prism spectra of late-type M, L and T dwarfs.⁶ The template sample was restricted to dwarfs later than M7 based on published optical classifications for M and L dwarfs (tied largely to the schemes of Kirkpatrick et al. 1991, 1999) and near-infrared classifications for T dwarfs (tied largely to the scheme of Burgasser et al. 2006b). About $\sim 15\%$ of the M and L dwarfs in our sample have only near-infrared types in the literature, based on various schemes (e.g., Reid et al. 2001a; Geballe et al. 2002). We also computed alternate near-infrared spectral classifications directly from the SpeX data using the Reid et al. (2001a) and Burgasser (2007a) index-spectral type relations, following the iterative procedure detailed in Burgasser et al. (2010). Known (resolved) binaries and sources noted to have peculiar spectra or highly uncertain classifications ($\sigma \geq \pm 2$ subtypes) were purged from the template sample. The resulting 462 spectra of 438 sources were interpolated onto a common wavelength scale, and synthetic Vega magnitudes in the five NICMOS filters and MKO⁷ *JHK_p* filters were computed by convolving each spectrum and a Kurucz model of Vega with the appropriate filter transmission functions (see Cushing et al. 2005).

From these individual templates, we produced separate libraries of binary templates for 2MASS J0850+1057 and 2MASS J1728+3948 by adding together appropriately scaled pairs. The pairs were initially selected to have secondary component types that were no more than 2 subtypes earlier than the primary type. This produced 137,212 unique combinations. We then computed an uncertainty-weighted mean relative flux scaling between the two components of each system using all five NICMOS measurements and *K_p* photometry⁸ from Konopacky et al. (2010); see Table 1. After scaling the spectra, we required that relative synthetic magnitudes in all six filter bands agree with measured values to within 3σ . This substantially reduced the number of “allowable” templates to 19,042 for 2MASS J0850+1057 and 1389 for 2MASS J1728+3948.

Comparisons were then made between the source spectral data and allowed binary templates using the weighted chi-squared statistic defined in Cushing et al.

⁶ These data were compiled from Burgasser et al. (2004, 2006a,b, 2007, 2008a,b, 2010); Cruz et al. (2004); Burgasser & McElwain (2006); Chiu et al. (2006); McElwain & Burgasser (2006); Reid et al. (2006); Burgasser (2007a,b,c); Liebert & Burgasser (2007); Looper et al. (2007, 2008b); Luhman et al. (2007); Siegler et al. (2007); Sheppard & Cushing (2009) and Schmidt et al. (2010a), and are available at the SpeX Prism Spectral Libraries website, <http://www.browndwarfs.org/spexprism>.

⁷ Mauna Kea Observatory filter system; see Tokunaga et al. (2002) and Simons & Tokunaga (2002).

⁸ Konopacky et al. (2010) also report resolved *J*- and *H*-band photometry for 2MASS J1728+3948, $\Delta J = 0.32 \pm 0.02$ and $\Delta H = 0.45 \pm 0.02$. These measurements are redundant—and in agreement—with broad-band F110W and F160W NICMOS photometry, and were therefore not used in the analysis.

(2008),

$$G_k \equiv \sum_{\{\lambda\}} w[\lambda] \left[\frac{D[\lambda] - \alpha T[\lambda]}{\sigma_D[\lambda]} \right]^2 \quad (2)$$

Here, $D[\lambda]$ and $T[\lambda]$ are the data and template spectra, respectively; $\sigma_D[\lambda]$ is the uncertainty spectrum of the data; $w[\lambda]$ is a vector of weights satisfying $\sum_{\{\lambda\}} w[\lambda] = 1$; α is a scaling factor that minimizes G_k (see Equation 2 in Cushing et al. 2008); and the sum is performed over the wavelength ranges $\{\lambda\} = 0.95\text{--}1.35 \mu\text{m}$, $1.45\text{--}1.8 \mu\text{m}$ and $2.0\text{--}2.35 \mu\text{m}$ to avoid regions of strong telluric absorption. We adopted the same weighting scheme as that used in Cushing et al. (2008) and Burgasser et al. (2010), with each pixel weighted by its spectral width (i.e., $w_i \equiv \Delta\lambda_i$).

Templates which provided minimum values of G_k were deemed to be the best fits. However, it was generally the case that other templates gave G_k values only slightly larger than this best-fit template, and are therefore statistically equivalent. We therefore determined average component parameters (spectral types and relative magnitudes) and their uncertainties following Burgasser et al. (2010, Equations 4–6), with an effective degrees of freedom $\nu = 253$ used for weighting the parameters with the F-test statistic.

4.2. Results

The resulting best-fitting binary templates are listed in Table 4, while Figures 4 and 5 display the four best fits to 2MASS J0850+1057 and 2MASS J1728+3948, respectively. These templates reproduce the observed data rather well, including the overall spectral slopes, shapes of the *JHK* flux peaks, and depths of the H₂O, CO and FeH absorption bands. By design, each of the spectral combinations listed also reproduce the relative magnitude measurements to within the observational uncertainties. Notably, the binary template fits are statistically superior to equivalent single template comparisons. Best-fit G_k values for these single templates were 2.20 for 2MASS J0850+1057 (comparing to the L5/L6.5⁹ 2MASSW J1326201-272937; Gizis 2002) and 3.90 for 2MASS J1728+3948 (comparing to the L5/L5 2MASS J06244595-4521548; Reid et al. 2008), differing at the $> 99.9\%$ significance level based on the F-test statistic. The significantly improved fits by the binary templates indicate that they are (as expected) better representations of the combined light spectra of these sources.

The spectra of the best-fit template components also replicate photometric trends from HST and LGSAO imaging. For 2MASS J0850+1057, each of the templates in Figure 4 has a secondary that is distinctly redder than its primary. These secondaries — 2MASSW J1553214+210907 (L5.5/L6.1; $J - K_s = 2.03 \pm 0.19$; Kirkpatrick et al. 1999), 2MASSI J0028394+150141 (L4.5/L5.2; $J - K_s = 1.95 \pm 0.13$; Kirkpatrick et al. 2000) and SDSSp J010752.33+004156.1 (L8/L6.0, $J - K_s = 2.12 \pm 0.07$; Geballe et al. 2002) are among the reddest L dwarfs currently known. In contrast, the primaries of these templates have $J - K_s$ colors that are in line with median values for their spectral types (e.g.,

⁹ Hereafter, we list both literature and SpeX spectral types for each template; uncertain types are indicated with “:” for ± 1 subtype, “:.” for ± 2 subtypes.

TABLE 4
 BEST FITTING BINARY TEMPLATES

Primary	SpT (Lit.) ^a	SpT (SpeX) ^b	Secondary	SpT (Lit.) ^a	SpT (SpeX) ^b	G_k	Relative Weight ^c
2MASS J08503593+1057156							
SDSS J151506.11+443648.3	L7.5±1.5 ^d	L6.9	2MASSW J1553214+210907	L5.5	L6.1:	1.46	1.00
SDSS J151506.11+443648.3	L7.5±1.5 ^d	L6.9	2MASSI J0028394+150141	L4.5	L5.2:.	1.57	0.28
SDSS J151506.11+443648.3	L7.5±1.5 ^d	L6.9	SDSSp J010752.33+004156.1	L8	L6.0	1.62	0.20
SDSS J171714.10+652622.2	L4	L5.8:	SDSSp J010752.33+004156.1	L8	L6.0	1.85	0.03
SDSS J171714.10+652622.2	L4	L5.8:	SDSS J080959.01+443422.2	L6 ^d	L6.2:	1.88	0.02
SDSS J171714.10+652622.2	L4	L5.8:	SDSSp J132629.82-003831.5	L8:	L6.1:	1.94	0.01
2MASS J03101401-2756452	L5	L6.0:	SDSSp J010752.33+004156.1	L8	L6.0	1.95	0.01
Weighted Mean	L7.5±0.0	L6.9±0.0	Weighted Mean	L5.7±1.2	L5.8±0.4
2MASS J17281150+3948593							
2MASS J01443536-0716142	L5	L3.9	SDSS J104409.43+042937.6	L7 ^d	L7.1	2.41	1.00
2MASSW J2224438-015852	L4.5	L4.0:	SDSS J104409.43+042937.6	L7 ^d	L7.1	2.58	0.29
2MASS J03185403-3421292	L7	L6.5	2MASS J09054654+5623117	L5	L5.6:	2.64	0.23
2MASS J01443536-0716142	L5	L3.9	2MASS J23254530+4251488	L8	L7.1	2.75	0.15
2MASS J03185403-3421292	L7	L6.5	2MASSI J1305410+204639	L4:	L6.0:	2.92	0.06
2MASS J01443536-0716142	L5	L3.9	SDSSp J003259.36+141036.6	L8 ^d	L7.9:	3.12	0.02
Weighted Mean	L5.3±1.0	L4.6±1.1	Weighted Mean	L6.5±1.1	L6.8±0.6

^a Optical spectral type from the literature unless otherwise noted.

^b Classifications based on H₂O and CH₄ index/spectral type relations defined in Burgasser (2007a), following the iterative procedure detailed in Burgasser et al. (2010).

^c Statistical weight assigned to template parameters in calculation of means and uncertainties. This weight corresponds to the F-test probability distribution function for the ratio $G_k/\min(G_k)$ and effective degrees of freedom $\nu = 211$ (see Equation 4 in Burgasser et al. 2010).

^d Near-infrared classification from the literature.

Schmidt et al. 2010b). What is more surprising, however, is that the best-fit secondaries are generally of *earlier type* than the best-fit primaries. This is true for both literature and SpeX classifications. The mean component classifications reflect this: L7.5 and L5.5±1.2 based on literature classifications and L7 and L6 based on SpeX classifications; we adopt the latter combination as the uncertainty-weighted means. This apparent reversal in classifications is particularly remarkable given the 0.8–1.2 magnitude brightness difference between the primary and secondary. There is no evidence that either component is a T dwarf.

For 2MASS J1728+3948, the best-fit secondaries are consistently bluer than the primaries, again in line with photometric trends. Notably, the components of the binaries shown in Figure 5 have comparable fluxes in the 0.9–1.0 μm region, supporting the F1042M flux reversal reported by Gizis et al. (2003), and diverge toward longer wavelengths. For these templates, it is the primary components that are unusually red: 2MASS J01443536-0716142 (L5/L4.2, $J - K_s = 1.92 \pm 0.03$; Liebert et al. 2003), 2MASSW J2224438-015852 (L4.5/L4.5:, $J - K_s = 2.05 \pm 0.04$; Kirkpatrick et al. 2000) and 2MASS J03185403-3421292 (L7/L6.4, $J - K_s = 2.06 \pm 0.07$; Kirkpatrick et al. 2008). The mean spectral type of 2MASS J1728+3948A, L5.5±1.0 from literature classifications and L4.5±1.1 from SpeX classifications, is also remarkable for being considerably earlier than the combined-light L7 optical classification. It is typically the earlier-type component that dominates optical flux in L and T dwarf binaries. In this case, it appears that the comparable brightnesses of the two components at red optical wavelengths produces a “blended” combined-light spectral type. The secondaries of the best-fit templates have normal colors, although both SDSS

J104409.43+042937.6 (L7/L6.9; Knapp et al. 2004) and 2MASS J23254530+4251488 (L8/L7.3:; Cruz et al. 2007) show weak signatures of 1.6 and 2.2 μm CH₄ absorption in their near-infrared spectra. These features suggest that 2MASS J1728+3948B is at the threshold of the L dwarf/T dwarf transition, despite its mid-L near-infrared spectral type. We adopt mean component types of L5 and L6.5 for this system.

4.3. Assessment of Systematic Effects

To assess the robustness of our results, we conducted the same template fits for three subsets of relative photometry: the NICMOS data alone, and single filter scalings with F110W and K_p photometry. The NICMOS fits produce little change in the inferred spectral components, with 2MASS J0850+1057 still hosting a later-type primary (L7 + L6 components based on both literature and SpeX classifications) and 2MASS J1728+3948 having a primary that is typed earlier than the combined light spectrum (L5 + L6.5 for literature classifications, L4 + L7 for SpeX classifications). However, the mean relative K_p magnitudes from these fits — 0.950±0.015 for 2MASS J0850+1057 and 0.54±0.05 for 2MASS J1728+3948 — differ from the measurements of Konopacky et al. (2010) at the 7σ and 1.5σ levels, respectively. Inferred brightnesses diverge even more dramatically when a single filter is used to scale the templates. F110W-scaled templates for 2MASS J0850+1057 indicate component types of L6 + L9:, with a significantly reduced best-fit G_k value (1.12 versus 1.46, distinct at the 98% confidence level). These types are more in line with prior estimates (e.g., Reid et al. 2001b), but the inferred component magnitudes differ significantly from measured values: $\Delta F160W$ disagrees at the 8σ level, while ΔK_p disagrees at the 6.5σ level. K_p

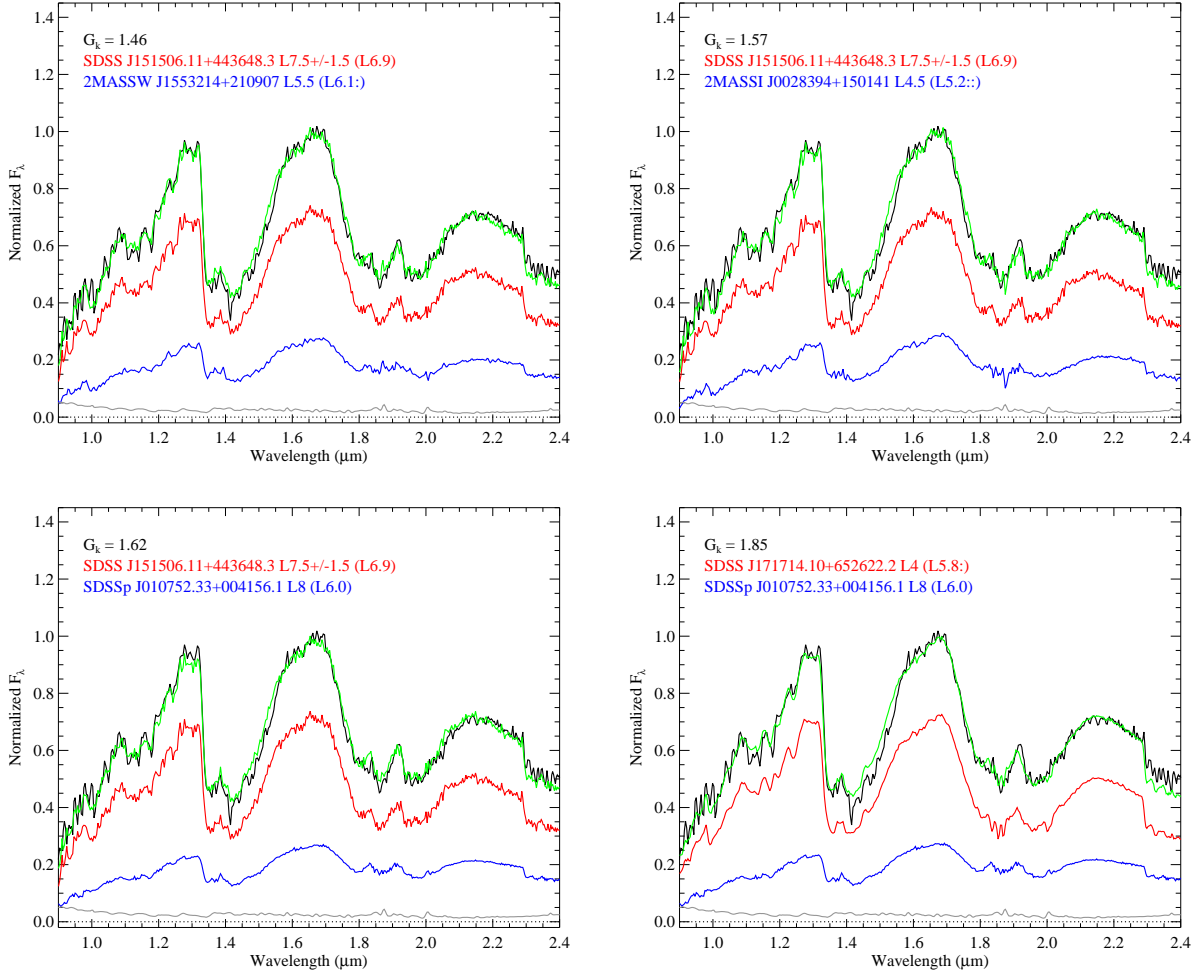


FIG. 4.— The four best template fits for 2MASS J0850+1057 as constrained by HST/NICMOS and LGSAO K_p photometry. In each panel, the source spectrum is indicated by the black line, the source noise spectrum by the grey line, the best-fitting template by the green line, the best-fitting primary by the red line and the best-fitting secondary by the blue line. Template spectra (and appropriately scaled primaries and secondaries) are shown at their minimum G_k scalings relative to the source spectrum, which is normalized at its peak spectral flux. Template source names, literature classifications, SpeX-based classifications (in parentheses) and G_k fit values are indicated. Note that the L7.5 \pm 1.5 literature spectral type for SDSS J151506.11+443648.3 is based on near-infrared data; all other literature types are based on optical data.

scaled templates for 2MASS J0850+1057 produce comparably large discrepancies in inferred NICMOS photometry. Single-filter template fits to 2MASS J1728+3948 are somewhat more robust, producing similar component types as the baseline template sample (L5+L7 for F110W fits, L5+L7.5: for K_p fits), although inferred relative magnitudes still deviate by up to 2σ .

We conclude that multi-band photometry is essential to accurately and precisely constrain the component properties of these binary systems, and particular care must be taken when drawing conclusions from single-filter measurements. Nevertheless, the general agreement in component types inferred from different multi-band subsets (e.g., NICMOS+ K_p , NICMOS only) indicates that our results are robust.

5. ABSOLUTE MAGNITUDE/SPECTRAL TYPES AND COLOR TRENDS

Both 2MASS J0850+1057 and 2MASS J1728+3948 have parallax distance measurements from Vrba et al. (2004), so it is possible to compare component absolute fluxes to those of comparable field dwarfs. Fig-

ure 6 displays combined light and component absolute MKO J and K magnitudes versus near-infrared spectral type and $J - K$ color. The MKO magnitudes from 2MASS J0850+1057 and 2MASS J1728+3948 are based on measurements from Leggett et al. (2002) for the former, and synthesized from 2MASS photometry and SpeX spectroscopy for the latter. Component JK fluxes were determined from the template fits, synthesized from the various best-fit template spectra and combined following the same weighting scheme as the average spectral types (Table 5). We use the near-infrared spectral types calculated in Section 2.2. The comparison sample was drawn from the compilation of Leggett et al. (2010), where we have either used published near-infrared spectral types listed in that study or types calculated from SpeX spectra (where available) following the same spectral index method described above.

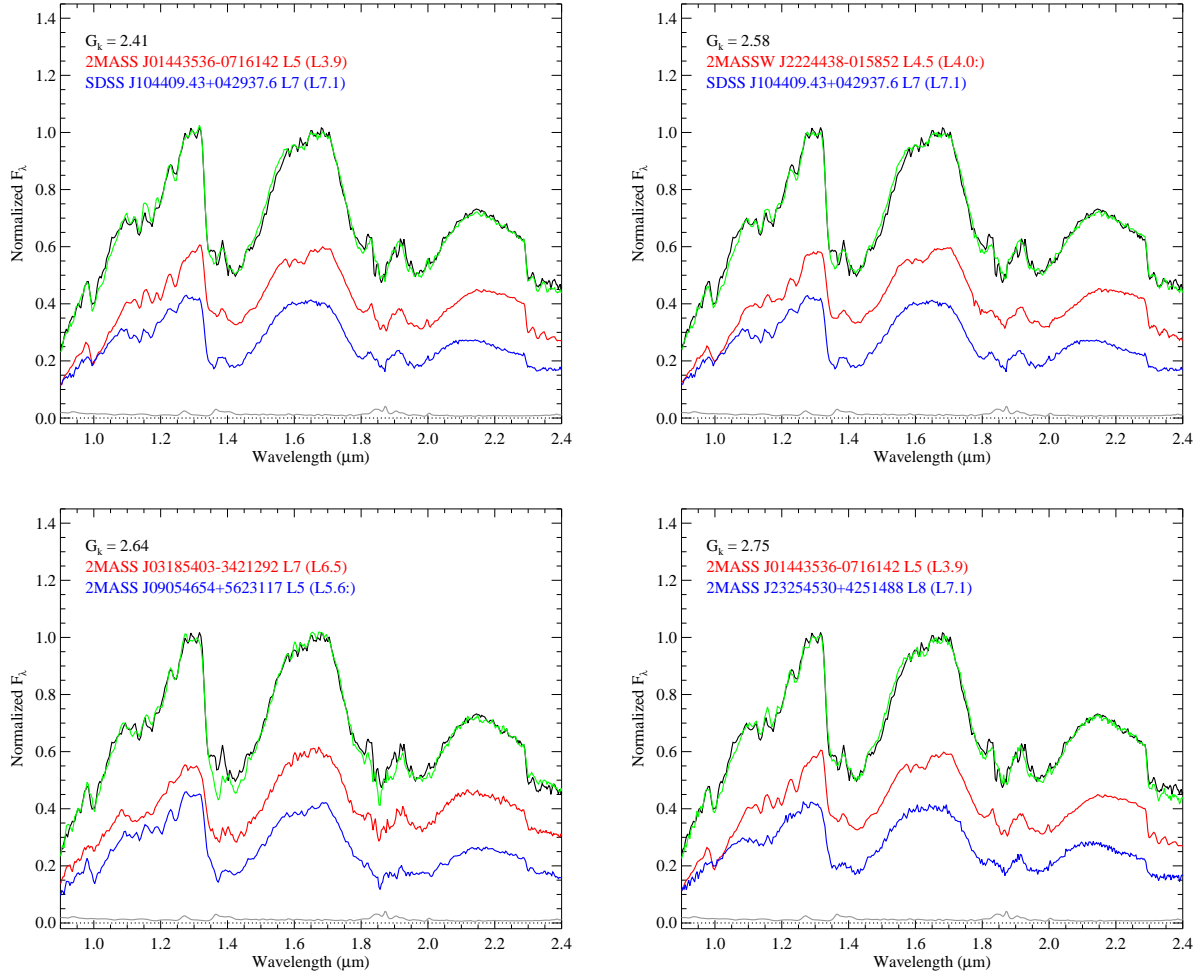


FIG. 5.— The four best template fits for 2MASS J1728+3948, displayed as in Figure 4. Note that the L7 literature spectral type for SDSS J104409.43+042937.6 is based on near-infrared data; all other literature types are based on optical data.

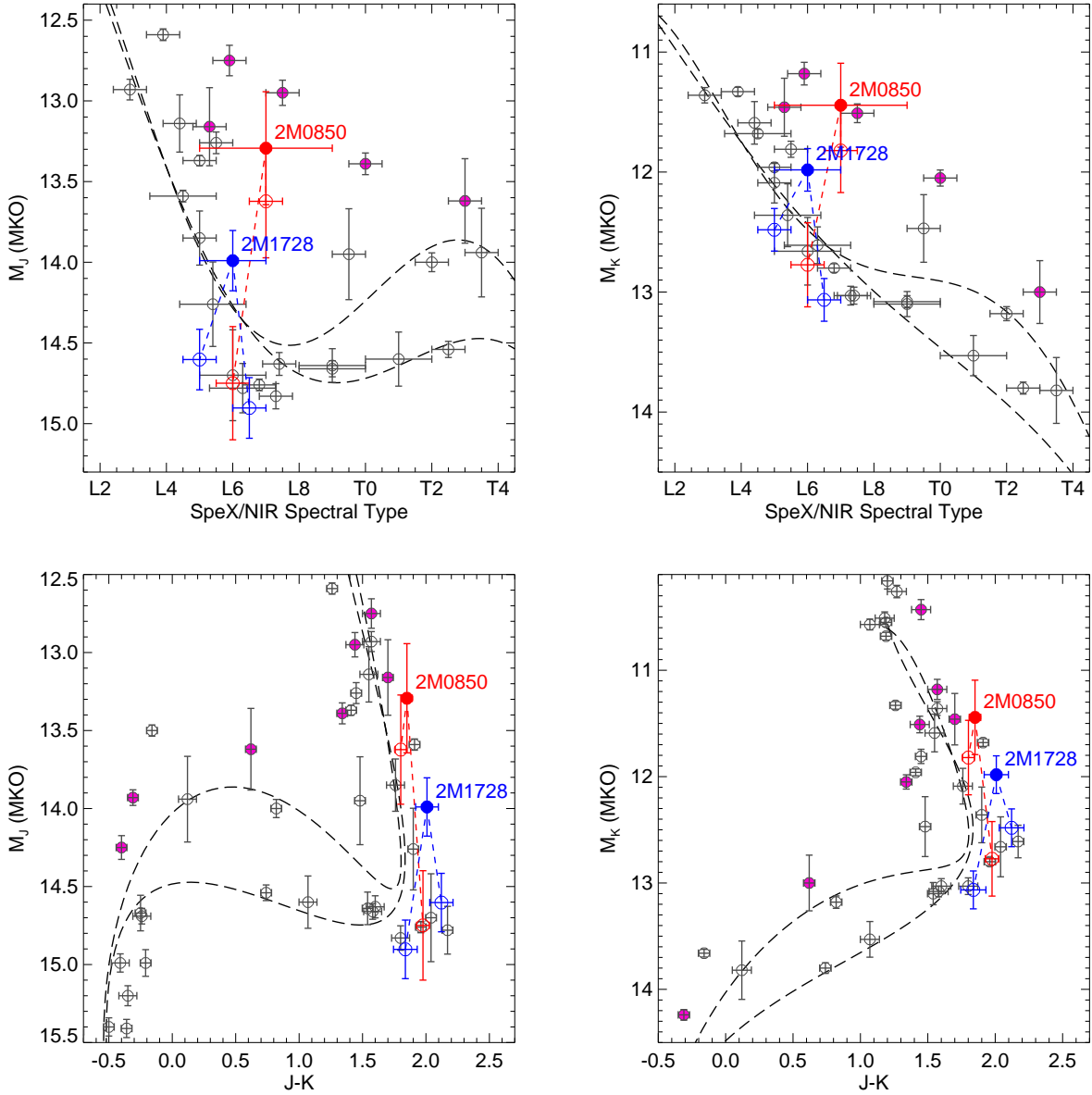


FIG. 6.— (Top panels) Absolute MKO J and K magnitudes versus spectral type for the 2MASS J0850+1057 (red) and 2MASS J1728+3948 (blue) components. These are compared to single (open symbols) and binary L and T dwarfs (filled symbols) with absolute magnitude uncertainties ≤ 0.3 mag, as compiled by Leggett et al. (2010). All sources are plotted according to their near-infrared classifications, either published or computed from SpeX spectroscopy. Also shown are the absolute magnitude/spectral type relations quantified in Liu et al. (2006, dashed lines); both “bright” and “faint” relations are shown. Combined light photometry for 2MASS J0850+1057 and 2MASS J1728+3948 are connected to component values. (Bottom panels) Absolute magnitudes versus MKO $J - K$ color based on the same sample.

Focusing first on the absolute magnitude/spectral type comparisons, we find that three of the components—2MASS J0850+1057B, 2MASS J1728+3948A and 2MASS J1728+3948B—roughly cluster, with absolute magnitudes similar to other L6–L8 sources. 2MASS J1728+3948A, and to a lesser degree 2MASS J1728+3948B, are somewhat underluminous for their types, particularly at J -band where they fall ≈ 0.5 mag below the absolute magnitude relations of Liu et al. (2006). In contrast, the primary of 2MASS J0850+1057 is ≈ 1 mag brighter than comparable L6–L8 dwarfs, or equivalently has a classification 3 subtypes too late for its measured absolute brightness. This component is even marginally brighter than combined light photometry for 2MASS J1728+3948. As such, the discrepancy between brightness and spectral type between the components of the 2MASS J0850+1057 system appears to be rooted to the unusually late spectral type and/or overluminosity of its primary.

In the near-infrared color-magnitude diagrams (CMDs), all four components follow the locus of field L dwarfs, tracing the inflection in $J - K$ color and M_J magnitude at the end of the L sequence. In particular, 2MASS J0850+1057B and 2MASS J1728+3948B bridge the turnover to bluer near-infrared colors, and the latter appears to be the faintest L dwarf with a parallax measurement currently known. Its location on the near-infrared CMDs supports our hypothesis that it is on the cusp of becoming a T dwarf (Section 4.2). The components of 2MASS J0850+1057 are no longer outliers in these plots, in contrast to prior results (e.g., Vrba et al. 2004). 2MASS J0850+1057A in particular does not stand out as unusually bright, due largely to the near-vertical locus of L dwarfs in near-infrared CMDs.

For completeness, we also determined luminosity, T_{eff} and mass estimates for the components of these binaries using their inferred absolute magnitudes and near-infrared spectral types. Bolometric luminosities were calculated using K -band bolometric corrections (BC_K) derived from the BC_K /spectral type relation of Dupuy & Liu (2009). Note that these values may be systematically too high for the unusually red sources 2MASS J0850+1057B and 2MASS J1728+3948A. T_{eff} s and masses were estimated using the Saumon & Marley (2008) cloudy evolutionary models, based on the derived luminosities and age estimates listed in Table 1; for 2MASS J1728+3948, we assumed an age range of 1.5–7.5 Gyr, the upper limit based on the small V_{tan} of this source. The inferred T_{eff} s for 2MASS J1728+3948A, 2MASS J0850+1057B and 2MASS J1728+3948B are consistent with prior estimates for L5–L6.5 dwarfs (Stephens et al. 2009), while the brightness of 2MASS J0850+1057A makes it ≈ 300 K warmer than comparable L7 dwarfs. We discuss this component in detail in Section 6.2.

6. DISCUSSION

6.1. Clouds and Classification

Our photometric and spectroscopic analyses of the components of 2MASS J0850+1057 and 2MASS J1728+3948 have revealed several unusual traits, particularly in their primaries: under- and overlu-

minous fluxes and unusually early and late near-infrared spectral types. These peculiar traits can be related to their unique atmospheric properties.

In the case of 2MASS J1728+3948A, we hypothesize that condensate cloud effects are responsible for shifting this component toward both an earlier near-infrared spectral classification and toward slightly fainter J -band fluxes. Grey extinction from condensate cloud grains in L dwarf photospheres dominate the opacity at the J - and H -band flux peaks, as these windows in molecular gas opacity probe deeper into the atmosphere and sample a larger column depth of cloud material (Ackerman & Marley 2001; Burrows et al. 2006). The K -band peak, on the other hand, is modulated by both cloud opacity and collision-induced H_2 absorption (Linsky 1969). As a result, greater condensate opacity tends to produce redder $J - K$ colors and fainter J -band fluxes (Allard et al. 2001; Marley et al. 2002; Tsuji et al. 2004). In addition, contrast in molecular absorption bands is reduced, particularly for the near-infrared H_2O and FeH bands to which near-infrared schemes are commonly tied (Reid et al. 2001a; Geballe et al. 2002). Veiling of these features can skew near-infrared classifications toward earlier types (Stephens 2003; Knapp et al. 2004). Hence, thicker condensate clouds leads to redder near-infrared colors, reduced flux at J -band, and systematically earlier near-infrared classifications.

These conditions accurately reflect the properties of 2MASS J1728+3948A, and to a lesser degree 2MASS J0850+1057B. The best-fit primary components for 2MASS J1728+3948 are consistently red, mid-type L dwarfs whose near-infrared spectral types are consistently earlier than their optical types (Table 4). These include the templates 2MASS J01443536-0716142 (hereafter 2MASS J0144-0716; L5 optical classification, L4 SpeX classification; Liebert et al. 2003) and 2MASSW J2224438-015852 (hereafter 2MASS J2224-0158; L4.5 optical classification, L3.5 near-infrared classification; Kirkpatrick et al. 2000; Knapp et al. 2004). Both of these sources exhibit indications of thick clouds, based on the detection of linear polarization in the case of 2MASS J0144-0716¹⁰ ($0.58 \pm 0.19\%$ at I -band; Zapatero Osorio et al. 2005), and spectral model fits and pronounced silicate grain absorption at 9–11 μm in the case of 2MASS J2224-0158 (Cushing et al. 2006, 2008; Stephens et al. 2009). Unusually red dwarfs such as these have been found to have cooler T_{eff} s for their spectral types (Stephens et al. 2009), which can contribute to fainter magnitudes. The older age of the 2MASS J1728+3948 system, based on the absence of Li I absorption, argues that thick condensate clouds, rather than low surface gravity, gives rise to its unusually red color (Allers et al. 2007; Loper et al. 2008b).

Thick clouds in 2MASS J1728+3948A may also explain its comparable brightness at 1 μm compared to its later-type companion. As discussed above, 2MASS J1728+3948B appears to be at the threshold of the L dwarf/T dwarf transition, a phase in which condensate clouds are inexplicably dispersed and J -band fluxes increase. In a sample of unresolved L/T transition binary candidates, Burgasser et al. (2010) found

¹⁰ 2MASS J0144-0716 was also detected in an optical flare by Liebert et al. (2003).

TABLE 5
ADOPTED COMPONENT PARAMETERS FOR 2MASS J08503593+1057156 AND
2MASS J17281150+3948593

Parameter	2MASS J0850+1057			2MASS J1728+3948	
	A	AA ^a	B	A	B
NIR Spectral Type	L7	L7+L7	L6	L5	L6.5
M_J	13.62±0.35	14.37±0.35	14.75±0.35	14.60±0.19	14.90±0.19
M_K	11.82±0.35	12.57±0.35	12.77±0.35	12.48±0.18	13.07±0.18
$J - K$	1.80±0.04	...	1.98±0.05	2.12±0.09	1.84±0.09
$\log L_{bol}/L_\odot$ ^b	-4.13±0.14	-4.43±0.14	-4.52±0.14	-4.42±0.08	-4.63±0.08
T_{eff} (K) ^c	1770±200	1480±180	1400±170	1570±80	1340±70
Mass (M_\odot) ^c	0.06±0.02	0.10±0.03	0.05±0.02	0.075±0.007	0.066±0.008

^a Parameters assuming two equal-mass components. Mass is given for combined pair.

^b Luminosity based on M_K magnitudes and K -band bolometric corrections (BC_K) from Dupuy & Liu (2009). Stated 1σ errors include ± 0.5 uncertainty in spectral type, absolute magnitude uncertainties, and 0.08 dex scatter in the Dupuy & Liu BC_K /spectral type relation.

^c T_{eff} and mass estimates based on inferred luminosities and ages listed in Table 1 (2MASS J1728+3948 is assumed to be 1.5–8 Gyr), combined with cloudy evolutionary models from Saumon & Marley (2008). Stated 1σ errors include uncertainties in luminosities and spread in age estimates.

that sources with comparable component types but redder primaries showed a more pronounced flux reversal than sources with normal or blue primaries. They argued that J -band fluxes in the primaries of these systems were more suppressed. We may be seeing a similar effect in the 2MASS J1728+3948AB pair. Alternatively, we may be observing the tops of thick clouds that are constrained to the same temperature layer in both sources (i.e., $T_{cr} = \text{constant}$; Tsuji 2005). These possibilities should be explored with detailed modeling of resolved component spectra, rather than spectral templates.

6.2. Is 2MASS J0850+1057 a Young Triplet?

While thick clouds can explain the unusual faintness of 2MASS J1728+3948A, thin clouds do not readily explain the unusual brightness of 2MASS J0850+1057A. Thin-cloud L dwarfs, also known as unusually blue L dwarfs (UBLs), do exhibit discrepancies between optical and near-infrared spectral types (Knapp et al. 2004; Burgasser et al. 2008b). There is also evidence that UBLs have systematically larger T_{eff} s and/or absolute fluxes for their spectral classifications (Stephens et al. 2009). However, 2MASS J0850+1057A has a normal near-infrared color for its spectral type, and best-fit templates exhibit none of the spectroscopic hallmarks of a UBL (e.g., deep H_2O and FeH bands, blue near-infrared SED; Burgasser et al. 2008b; Schmidt et al. 2010a). It is therefore unlikely that this source is a UBL with unusually thin clouds.

Youth may play a role in the unusual brightness of 2MASS J0850+1057A, arising from the enlarged radius of a still-contracting brown dwarf. The radius of a 1500 K brown dwarf is 25% larger at an age of 250 Myr — the minimum bound cited by Faherty et al. (2010) — than at 2 Gyr, corresponding to an increase in brightness of roughly 0.5 mag. Given the current uncertainties in the distance of this source, such a shift may be sufficient to move 2MASS J0850+1057A back onto absolute magnitude/spectral type tracks. However, assuming that the two components of this system are coeval, 2MASS J0850+1057B would also have to be overluminous by roughly the same factor, which does not appear

to be the case. Moreover, such a correction fails to explain the significant brightness difference between these two comparably-classified sources.

We propose an alternative explanation: 2MASS J0850+1057A is itself an unresolved, near-equal mass binary. Such a scenario would explain how this component could appear both brighter and warmer than its equivalently-typed companion, but have an otherwise normal spectral energy distribution. The components of an equal-mass 2MASS J0850+1057A pair would have absolute magnitudes, luminosities and T_{eff} s fully consistent with empirical trends (Table 5). The fact that existing high angular resolution images have not resolved this source requires an angular separation $\lesssim 50$ –100 mas, or a projected separation $\lesssim 2$ –4 pc at this distance of this system. In fact, long-term dynamic stability requires an even tighter binary. A hierarchical triple is generally stable if the ratio of outer periastron and inner apastron distances:

$$Y \equiv \frac{a_{out}(1 - e_{out})}{a_{in}(1 + e_{in})} \quad (3)$$

satisfies

$$Y > Y^{min} \equiv 1 + \frac{3.7}{q_{out}^{1/3}} + \frac{2.2}{q_{out}^{1/3} + 1} + \frac{1.4}{q_{in}^{1/3}} \frac{q_{out}^{1/3} - 1}{q_{out}^{1/3} + 1}. \quad (4)$$

(Eggleton & Kiseleva 1995). Here, $q_{in} \equiv \frac{M_1}{M_2} \geq 1$ and $q_{out} \equiv \frac{M_1 + M_2}{M_3}$ are the inner and outer mass ratios. Assuming that all three components have nearly equal masses, and that the inner and outer orbits have eccentricities $e = 0$ (0.5), Equation 4 requires a limit on the inner orbit semimajor axis of $a_{in} < 0.2a_{out}$ ($< 0.07a_{out}$) and hence $a_{in} < 25$ mas (8 mas), or 1 AU (0.3 AU), based on the semimajor axis determination of Konopacky et al. (2010) and the Vrba et al. (2004) parallax.

Such a tight separation is not unusual for brown dwarf multiples; brown dwarf spectroscopic binaries with comparable separations have already been identified (e.g., Basri & Martín 1999; Blake et al. 2008; Joergens et al. 2010). Moreover, three other tight, hi-

erarchical, brown dwarf triple candidates identified in the literature—Gliese 569BCD, (Simon et al. 2006), DENIS J0205-1159ABC (Bouy et al. 2005), and Kelu 1ABC (Stumpf et al. 2010)—exhibit evidence that one component is an unresolved pair, based on radial velocity variations, PSF-fitting residuals and spectroscopic features, respectively. This scenario is also consistent with orbital mass constraints from Konopacky et al. (2010), as the estimated total mass of a triple 2MASS J0850+1057 system, $0.15 \pm 0.04 M_{\odot}$, is closer to the mean (but weakly constrained) value of $0.2 M_{\odot}$ found in that study. Indeed, tighter constraints on the total mass of this system from ongoing astrometric monitoring may affirm or refute the presence of a third body. The triple hypothesis can also be tested through radial velocity monitoring; a $\lesssim 5 \text{ km s}^{-1}$ ($\lesssim 8 \text{ km s}^{-1}$) line shift arising from a pair of $0.05 M_{\odot}$ brown dwarfs separated by 1.0 AU (0.3 AU) can be readily detected with current near-infrared instrumentation (Blake et al. 2007; Bean et al. 2010).

If 2MASS J0850+1057A is confirmed as a binary, it would complete a remarkable, young, low-mass, hierarchical quintuple system with the double M dwarf NLTT 20346AB, encompassing 4 orders of magnitude in separation and composed entirely of objects less massive than $0.15 M_{\odot}$ (Faherty et al. 2010).

7. SUMMARY

We have presented photometric and spectroscopic analyses of the late-type L dwarf binaries 2MASS J0850+1057 and 2MASS J1728+3948, aimed at assessing component spectral types, absolute magnitudes and near-infrared colors. Multi-band HST/NICMOS photometry have revealed distinct trends in the relative colors of these two systems, with 2MASS J0850+1057B being redder than its primary and 2MASS J1728+3948B being bluer. Neither secondary exhibits narrow-band colors consistent with being a T dwarf. These results are borne out in spectral template fits, using NICMOS and K_p resolved photometry, which also determine component near-infrared spectral types of L7 + L6 for 2MASS J0850+1057 and L5 + L6.5 for 2MASS J1728+3948. The early classification of 2MASS J1728+3948A, its relative faintness at J , and its unusually red color can be explained by the presence of thick condensate clouds in its photosphere. The secondary of this system, in contrast, may be losing its photospheric cloud deck as it transitions onto the T dwarf sequence. For 2MASS J0850+1057, the surprisingly later spectral type of its bright primary may stem from youth (inflated radius) and/or unresolved multiplicity. The latter hypothesis, which would make 2MASS J0850+1057 part of a low-mass hierarchical quintuple, can be tested through ongoing astrometric monitoring and/or resolved spectroscopic monitoring to search for RV variations.

As two resolved (or partly-resolved) coeval systems spanning the end of the L dwarf sequence and exhibiting a broad range of cloud properties, 2MASS J0850+1057 and 2MASS J1728+3948 remain important laboratories for studying cloud formation and evolution in low-temperature atmospheres. Improved parallactic distance measurements—including resolution of current distance discrepancies for 2MASS J0850+1057—resolved component spectroscopy, and ongoing photometric and astro-

metric monitoring will aid in characterizing the clouds, spectral properties and multiplicity of these benchmark brown dwarf systems.

The authors would like to thank telescope operators Dave Griep and Bill Grolisch and instrument specialist John Rayner for their assistance during the IRTF observations. We acknowledge helpful comments from Trent Dupuy and Jacqueline Faherty on our original manuscript, and thank our referee Sandy Leggett for her prompt and helpful review. AJB acknowledges support from the Chris and Warren Hellman Fellowship; DCBG acknowledges funding from the John Reed Fund. This publication makes use of data from the Two Micron All Sky Survey, which is a joint project of the University of Massachusetts and the Infrared Processing and Analysis Center, and funded by the National Aeronautics and Space Administration and the National Science Foundation. 2MASS data were obtained from the NASA/IPAC Infrared Science Archive, which is operated by the Jet Propulsion Laboratory, California Institute of Technology, under contract with the National Aeronautics and Space Administration. This research has also made use of the SIMBAD database, operated at CDS, Strasbourg, France; the M, L, and T dwarf compendium housed at DwarfArchives.org and maintained by Chris Gelino, Davy Kirkpatrick, and Adam Burgasser; the SpeX Prism Spectral Libraries, maintained by Adam Burgasser at <http://www.browndwarfs.org/spexprism>; and the VLM Binaries Archive maintained by Nick Siegler at <http://www.vlmbinaries.org>. The authors wish to recognize and acknowledge the very significant cultural role and reverence that the summit of Mauna Kea has always had within the indigenous Hawaiian community. We are most fortunate to have the opportunity to conduct observations from this mountain.

Facilities: IRTF (SpeX), Hubble Space Telescope (NICMOS)

REFERENCES

- Ackerman, A. S., & Marley, M. S. 2001, *ApJ*, 556, 872
- Allard, F., Hauschildt, P. H., Alexander, D. R., Tamanaï, A., & Schweitzer, A. 2001, *ApJ*, 556, 357
- Allen, P. R. 2007, *ApJ*, 668, 492
- Allers, K. N., Jaffe, D. T., Luhman, K. L., Liu, M. C., Wilson, J. C., Skrutskie, M. F., Nelson, M., Peterson, D. E., Smith, J. D., & Cushing, M. C. 2007, *ApJ*, 657, 511
- Artigau, É., Bouchard, S., Doyon, R., & Lafrenière, D. 2009, *ApJ*, 701, 1534
- Bailer-Jones, C. A. L., & Mundt, R. 2001, *A&A*, 367, 218
- Basri, G., & Martín, E. L. 1999, *AJ*, 118, 2460
- Bean, J. L., Seifahrt, A., Hartman, H., Nilsson, H., Reiners, A., Dreizler, S., Henry, T. J., & Wiedemann, G. 2010, *ApJ*, 711, L19
- Blake, C. H., Charbonneau, D., White, R. J., Marley, M. S., & Saumon, D. 2007, *ApJ*, 666, 1198
- Blake, C. H., Charbonneau, D., White, R. J., Torres, G., Marley, M. S., & Saumon, D. 2008, *ApJ*, 678, L125
- Bouy, H., Brandner, W., Martín, E. L., Delfosse, X., Allard, F., & Basri, G. 2003, *AJ*, 126, 1526
- Bouy, H., Martín, E. L., Brandner, W., & Bouvier, J. 2005, *AJ*, 129, 511
- Bouy, H., Martín, E. L., Brandner, W., Forveille, T., Delfosse, X., Huéramo, N., Basri, G., Girard, J., Zapatero Osorio, M.-R., Stumpf, M., Ghez, A., Valdivielso, L., Marchis, F., Burgasser, A. J., & Cruz, K. 2008, *A&A*, 481, 757
- Burgasser, A. J. 2007a, *ApJ*, 659, 655
- , 2007b, *AJ*, 134, 1330
- , 2007c, *ApJ*, 658, 617
- Burgasser, A. J., Burrows, A., & Kirkpatrick, J. D. 2006a, *ApJ*, 639, 1095
- Burgasser, A. J., Cruz, K. L., Cushing, M., Gelino, C. R., Looper, D. L., Faherty, J. K., Kirkpatrick, J. D., & Reid, I. N. 2010, *ApJ*, 710, 1142
- Burgasser, A. J., Geballe, T. R., Leggett, S. K., Kirkpatrick, J. D., & Golimowski, D. A. 2006b, *ApJ*, 637, 1067
- Burgasser, A. J., Kirkpatrick, J. D., Cruz, K. L., Reid, I. N., Leggett, S. K., Liebert, J., Burrows, A., & Brown, M. E. 2006c, *ApJS*, 166, 585
- Burgasser, A. J., Liu, M. C., Ireland, M. J., Cruz, K. L., & Dupuy, T. J. 2008a, *ApJ*, 681, 579
- Burgasser, A. J., Looper, D. L., Kirkpatrick, J. D., Cruz, K. L., & Swift, B. J. 2008b, *ApJ*, 674, 451
- Burgasser, A. J., Looper, D. L., Kirkpatrick, J. D., & Liu, M. C. 2007, *ApJ*, 658, 557
- Burgasser, A. J., Marley, M. S., Ackerman, A. S., Saumon, D., Lodders, K., Dahn, C. C., Harris, H. C., & Kirkpatrick, J. D. 2002, *ApJ*, 571, L151
- Burgasser, A. J., & McElwain, M. W. 2006, *AJ*, 131, 1007
- Burgasser, A. J., McElwain, M. W., Kirkpatrick, J. D., Cruz, K. L., Tinney, C. G., & Reid, I. N. 2004, *AJ*, 127, 2856
- Burningham, B., et al. 2008, *MNRAS*, 391, 320
- Burrows, A., Marley, M., Hubbard, W. B., Lunine, J. I., Guillot, T., Saumon, D., Freedman, R., Sudarsky, D., & Sharp, C. 1997, *ApJ*, 491, 856
- Burrows, A., Marley, M. S., & Sharp, C. M. 2000, *ApJ*, 531, 438
- Burrows, A., Sudarsky, D., & Hubeny, I. 2006, *ApJ*, 640, 1063
- Bushouse, H. 1997, in *The 1997 HST Calibration Workshop with a New Generation of Instruments*, p. 223, ed. S. Casertano, R. Jedrzejewski, T. Keyes, & M. Stevens, 223+
- Chiu, K., Fan, X., Leggett, S. K., Golimowski, D. A., Zheng, W., Geballe, T. R., Schneider, D. P., & Brinkmann, J. 2006, *AJ*, 131, 2722
- Cruz, K. L., Burgasser, A. J., Reid, I. N., & Liebert, J. 2004, *ApJ*, 604, L61
- Cruz, K. L., Reid, I. N., Kirkpatrick, J. D., Burgasser, A. J., Liebert, J., Solomon, A. R., Schmidt, S. J., Allen, P. R., Hawley, S. L., & Covey, K. R. 2007, *AJ*, 133, 439
- Cushing, M. C., Marley, M. S., Saumon, D., Kelly, B. C., Vacca, W. D., Rayner, J. T., Freedman, R. S., Lodders, K., & Roellig, T. L. 2008, *ApJ*, 678, 1372
- Cushing, M. C., Rayner, J. T., & Vacca, W. D. 2005, *ApJ*, 623, 1115
- Cushing, M. C., Roellig, T. L., Marley, M. S., Saumon, D., Leggett, S. K., Kirkpatrick, J. D., Wilson, J. C., Sloan, G. C., Mainzer, A. K., Van Cleve, J. E., & Houck, J. R. 2006, *ApJ*, 648, 614
- Cushing, M. C., Vacca, W. D., & Rayner, J. T. 2004, *PASP*, 116, 362
- Dahn, C. C., Harris, H. C., Vrba, F. J., Guetter, H. H., Canzian, B., Henden, A. A., Levine, S. E., Luginbuhl, C. B., Monet, A. K. B., Monet, D. G., Pier, J. R., Stone, R. C., Walker, R. L., Burgasser, A. J., Gizis, J. E., Kirkpatrick, J. D., Liebert, J., & Reid, I. N. 2002, *AJ*, 124, 1170
- Dupuy, T. J., & Liu, M. C. 2009, *ApJ*, 704, 1519
- Eggleton, P., & Kiseleva, L. 1995, *ApJ*, 455, 640
- Faherty, J. K., Burgasser, A. J., Bochanski, J. J., Looper, D. L., & West, A. A. 2010, *Astronomical Journal*, submitted
- Fortney, J. J. 2005, *MNRAS*, 364, 649
- Geballe, T. R., Knapp, G. R., Leggett, S. K., Fan, X., Golimowski, D. A., Anderson, S., Brinkmann, J., Csabai, I., Gunn, J. E., Hawley, S. L., Hennessy, G., Henry, T. J., Hill, G. J., Hindsley, R. B., Ivezić, Z., Lupton, R. H., McDaniel, A., Munn, J. A., Narayanan, V. K., Peng, E., Pier, J. R., Rockosi, C. M., Schneider, D. P., Smith, J. A., Strauss, M. A., Tsvetanov, Z. I., Uomoto, A., York, D. G., & Zheng, W. 2002, *ApJ*, 564, 466
- Gelino, C. R., Marley, M. S., Holtzman, J. A., Ackerman, A. S., & Lodders, K. 2002, *ApJ*, 577, 433
- Gizis, J. E. 2002, *ApJ*, 575, 484
- Gizis, J. E., Reid, I. N., Knapp, G. R., Liebert, J., Kirkpatrick, J. D., Koerner, D. W., & Burgasser, A. J. 2003, *AJ*, 125, 3302
- Golimowski, D. A., et al. 2004, *AJ*, 127, 3516
- Helling, C., Dehn, M., Woitke, P., & Hauschildt, P. H. 2008, *ApJ*, 675, L105
- Helling, C., & Woitke, P. 2006, *A&A*, 455, 325
- Joergens, V., Mueller, A., & Reffert, S. 2010, *ArXiv e-prints*
- Kirkpatrick, J. D. 2005, *ARA&A*, 43, 195
- Kirkpatrick, J. D., Henry, T. J., & McCarthy, Jr., D. W. 1991, *ApJS*, 77, 417
- Kirkpatrick, J. D., Reid, I. N., Liebert, J., Cutri, R. M., Nelson, B., Beichman, C. A., Dahn, C. C., Monet, D. G., Gizis, J. E., & Skrutskie, M. F. 1999, *ApJ*, 519, 802
- Kirkpatrick, J. D., Reid, I. N., Liebert, J., Gizis, J. E., Burgasser, A. J., Monet, D. G., Dahn, C. C., Nelson, B., & Williams, R. J. 2000, *AJ*, 120, 447
- Kirkpatrick, J. D., et al. 2008, *ApJ*, 689, 1295
- Knapp, G. R., Leggett, S. K., Fan, X., Marley, M. S., Geballe, T. R., Golimowski, D. A., Finkbeiner, D., Gunn, J. E., Hennawi, J., Ivezić, Z., Lupton, R. H., Schlegel, D. J., Strauss, M. A., Tsvetanov, Z. I., Chiu, K., Hoversten, E. A., Glazebrook, K., Zheng, W., Hendrickson, M., Williams, C. C., Uomoto, A., Vrba, F. J., Henden, A. A., Luginbuhl, C. B., Guetter, H. H., Munn, J. A., Canzian, B., Schneider, D. P., & Brinkmann, J. 2004, *AJ*, 127, 3553
- Koen, C. 2003, *MNRAS*, 346, 473
- Konopacky, Q. M., Ghez, A. M., Barman, T. S., Rice, E. L., Bailey, J. I., White, R. J., McLean, I. S., & Duchêne, G. 2010, *ApJ*, 711, 1087
- Krist, J. 1995, in *Astronomical Society of the Pacific Conference Series*, Vol. 77, *Astronomical Data Analysis Software and Systems IV*, ed. R. A. Shaw, H. E. Payne, & J. J. E. Hayes, 349+
- Leggett, S. K., Burningham, B., Saumon, D., Marley, M. S., Warren, S. J., Smart, R. L., Jones, H. R. A., Lucas, P. W., Pinfield, D. J., & Tamura, M. 2010, *ApJ*, 710, 1627
- Leggett, S. K., Geballe, T. R., Fan, X., Schneider, D. P., Gunn, J. E., Lupton, R. H., Knapp, G. R., Strauss, M. A., McDaniel, A., Golimowski, D. A., Henry, T. J., Peng, E., Tsvetanov, Z. I., Uomoto, A., Zheng, W., Hill, G. J., Ramsey, L. W., Anderson, S. F., Annis, J. A., Bahcall, N. A., Brinkmann, J., Chen, B., Csabai, I., Fukugita, M., Hennessy, G. S., Hindsley, R. B., Ivezić, Z., Lamb, D. Q., Munn, J. A., Pier, J. R., Schlegel, D. J., Smith, J. A., Stoughton, C., Thakar, A. R., & York, D. G. 2000, *ApJ*, 536, L35
- Leggett, S. K., et al. 2002, *ApJ*, 564, 452
- Liebert, J., & Burgasser, A. J. 2007, *ApJ*, 655, 522

- Liebert, J., Kirkpatrick, J. D., Cruz, K. L., Reid, I. N., Burgasser, A., Tinney, C. G., & Gizis, J. E. 2003, *AJ*, 125, 343
- Linsky, J. L. 1969, *ApJ*, 156, 989
- Liu, M. C., Leggett, S. K., Golimowski, D. A., Chiu, K., Fan, X., Geballe, T. R., Schneider, D. P., & Brinkmann, J. 2006, *ApJ*, 647, 1393
- Lodders, K., & Fegley, B. 2002, *Icarus*, 155, 393
- Looper, D. L., Gelino, C. R., Burgasser, A. J., & Kirkpatrick, J. D. 2008a, *ApJ*, 685, 1183
- Looper, D. L., Kirkpatrick, J. D., & Burgasser, A. J. 2007, *AJ*, 134, 1162
- Looper, D. L., Kirkpatrick, J. D., Cutri, R. M., Barman, T., Burgasser, A. J., Cushing, M. C., Roellig, T., McGovern, M. R., McLean, I. S., Rice, E., Swift, B. J., & Schurr, S. D. 2008b, *ApJ*, 686, 528
- Luhman, K. L., et al. 2007, *ApJ*, 654, 570
- Magazzu, A., Martin, E. L., & Rebolo, R. 1993, *ApJ*, 404, L17
- Marley, M. S., Seager, S., Saumon, D., Lodders, K., Ackerman, A. S., Freedman, R. S., & Fan, X. 2002, *ApJ*, 568, 335
- McElwain, M. W., & Burgasser, A. J. 2006, *AJ*, 132, 2074
- McLean, I. S., McGovern, M. R., Burgasser, A. J., Kirkpatrick, J. D., Prato, L., & Kim, S. S. 2003, *ApJ*, 596, 561
- Oppenheimer, B. R., Kulkarni, S. R., Matthews, K., & Nakajima, T. 1995, *Science*, 270, 1478
- Rayner, J. T., Toomey, D. W., Onaka, P. M., Denault, A. J., Stahlberger, W. E., Vacca, W. D., Cushing, M. C., & Wang, S. 2003, *PASP*, 115, 362
- Rebolo, R., Martin, E. L., & Magazzu, A. 1992, *ApJ*, 389, L83
- Reid, I. N., Burgasser, A. J., Cruz, K. L., Kirkpatrick, J. D., & Gizis, J. E. 2001a, *AJ*, 121, 1710
- Reid, I. N., Cruz, K. L., Kirkpatrick, J. D., Allen, P. R., Mungall, F., Liebert, J., Lowrance, P., & Sweet, A. 2008, *AJ*, 136, 1290
- Reid, I. N., Gizis, J. E., Kirkpatrick, J. D., & Koerner, D. W. 2001b, *AJ*, 121, 489
- Reid, I. N., Lewitus, E., Burgasser, A. J., & Cruz, K. L. 2006, *ApJ*, 639, 1114
- Roellig, T. L., Van Cleve, J. E., Sloan, G. C., Wilson, J. C., Saumon, D., Leggett, S. K., Marley, M. S., Cushing, M. C., Kirkpatrick, J. D., Mainzer, A. K., & Houck, J. R. 2004, *ApJS*, 154, 418
- Saumon, D., & Marley, M. S. 2008, *ApJ*, 689, 1327
- Saumon, D., Marley, M. S., Cushing, M. C., Leggett, S. K., Roellig, T. L., Lodders, K., & Freedman, R. S. 2006, *ApJ*, 647, 552
- Schmidt, S. J., West, A. A., Burgasser, A. J., Bochanski, J. J., & Hawley, S. L. 2010a, *AJ*, 139, 1045
- Schmidt, S. J., West, A. A., Hawley, S. L., & Pineda, J. S. 2010b, *AJ*, 139, 1808
- Sheppard, S. S., & Cushing, M. C. 2009, *AJ*, 137, 304
- Siegler, N., Close, L. M., Burgasser, A. J., Cruz, K. L., Marois, C., Macintosh, B., & Barman, T. 2007, *AJ*, 133, 2320
- Simon, M., Bender, C., & Prato, L. 2006, *ApJ*, 644, 1183
- Simons, D. A., & Tokunaga, A. 2002, *PASP*, 114, 169
- Skrutskie, M. F., et al. 2006, *AJ*, 131, 1163
- Stephens, D. C. 2003, in *IAU Symposium*, Vol. 211, *Brown Dwarfs*, ed. E. Martín, 355–+
- Stephens, D. C., Leggett, S. K., Cushing, M. C., Marley, M. S., Saumon, D., Geballe, T. R., Golimowski, D. A., Fan, X., & Noll, K. S. 2009, *ApJ*, 702, 154
- Stumpf, M. B., Brandner, W., Henning, T., Bouy, H., Koehler, R., Hormuth, F., Joergens, V., & Kasper, M. 2010, *Astronomy and Astrophysics*, in press
- Tinney, C. G., Burgasser, A. J., & Kirkpatrick, J. D. 2003, *AJ*, 126, 975
- Tody, D. 1986, in *Society of Photo-Optical Instrumentation Engineers (SPIE) Conference Series*, Vol. 627, *Society of Photo-Optical Instrumentation Engineers (SPIE) Conference Series*, ed. D. L. Crawford, 733–+
- Tokunaga, A. T., Simons, D. A., & Vacca, W. D. 2002, *PASP*, 114, 180
- Tsuji, T. 2005, *ApJ*, 621, 1033
- Tsuji, T., Nakajima, T., & Yanagisawa, K. 2004, *ApJ*, 607, 511
- Vacca, W. D., Cushing, M. C., & Rayner, J. T. 2003, *PASP*, 115, 389
- Vrba, F. J., Henden, A. A., Luginbuhl, C. B., Guetter, H. H., Munn, J. A., Canzian, B., Burgasser, A. J., Kirkpatrick, J. D., Fan, X., Geballe, T. R., Golimowski, D. A., Knapp, G. R., Leggett, S. K., Schneider, D. P., & Brinkmann, J. 2004, *AJ*, 127, 2948
- Yamamura, I., Tsuji, T., & Tanabe, T. 2010, *ArXiv e-prints*
- Zapatero Osorio, M. R., Caballero, J. A., & Béjar, V. J. S. 2005, *ApJ*, 621, 445